PERGAMON

International Journal of Solids and Structures 37 (2000) 5385–5411

INTERNATIONAL JOURNAL OF SOLIDS and STRUCTURES

www.elsevier.com/locate/ijsolstr

The effect of yield strength mis-match on the fracture analysis of welded joints: slip-line field solutions for pure bending

S. Hao, K.-H. Schwalbe*, A. Cornec

Institut fur Werksrofforschung, Max-Plank-Strasse, GKSS-Forschungszentrum Geesthacht, Geesthacht, Germany

Received 31 October 1996; in revised form 31 August 1999

Abstract

Plane strain and plane stress slip-line solutions for single notched bending specimens with a central mismatched welded joint have been derived. The crack has been located on the fusion line (interface) and at the middle of the weld metal. 2D and 3D finite element analysis has been performed to verify the theoretical results and to investigate the effect of specimen thickness. From these solutions, the stress distribution and deformation field in the weld metal, the expressions for the yield load as well as the constraint state at the crack tip are determined. The resulting relations for estimating 3D effects coincide with the test results. © 2000 Elsevier Science Ltd. All rights reserved.

Keywords: Welded joints; Slip-line field analysis; Yield strength mis-match; Yield moment; Constraint

1. Introduction

It is well known that material heterogeneity, such as represented by a mismatched welded joint in an engineering structure, may have strong effects on fracture behavior. 'Mis-match' means that weld metal and base material are different in yield stress; this can be described by the parameter M:

$$M = \frac{\sigma_{YW}}{\sigma_{YB}} \tag{1}$$

where σ_{YW} and σ_{YB} are the yield stress of the weld metal and the base material, respectively. $M < 1$ refers to undermatching, $M > 1$ represents overmatching.

* Corresponding author. Fax: +49-4152-87-2534.

PII: S0020-7683(99)00246-2

Nomenclature

a	crack length for SENB specimen or half crack length for CCT specimen
B	thickness of welded joint
E	elastic modulus
F	applied load for unit thickness
H	half height of weld metal strip
k_B, k_W	shear yield stress of base (B) and weld (W) material, respectively
M	mismatch factor, $M = \sigma_{YW}/\sigma_{YB}$
MF	applied moment for unit thickness
MF_Y	yield moment for a homogeneous specimen with unit thickness
MF_{YL}	moment characterising the beginning of local yielding, per unit thickness
MF_{YM}	yield moment of a mismatched welded joint, per unit thickness
MF_{YB}	yield moment of an all-base material specimen, per unit thickness
MF_{YW}	yield moment of an all-weld material specimen, per unit thickness
N_B, N_W	hardening exponents of base (B) and weld (W) material, respectively
N_{M1}	mismatching hardening exponents at net-section yielding stage
r, φ	polar coordinates
x_1, x_2	Cartesian coordinates
u_i,	displacement components ($i = 1, 2$)
v_i,	velocity components ($i = 1, 2$)
Q	constraint parameter at crack tip
T_i	traction force on a body surface
V_p	plastic component of CMOD
W	width of SENB specimen
ε_{ij}	strain components; $i, j = 1, 2$ (Cartesian coordinates), $i, j = r, \varphi$ (polar coordinates)
θ	angle between an α slip-line group and the horizontal direction
φ, r	polar co-ordinates
σ_e	equivalent von Mises stress
σ_{ij}	stress components; $i, j = 1, 2$ (Cartesian coordinates), $i, j = r, \varphi$ (polar coordinates)
σ_m	mean stress: $\sigma_m = (\sigma_{11} + \sigma_{22})/2$; in plane strain condition, σ_m equals the triaxial stress: $\sigma_m = \sigma_{ij}\delta_{ij}/3$
σ_Y	yield stress
σ_{YB}, σ_{YW}	yield stress of base (B) and weld (W) material, respectively
ν	Poisson's ratio
CCT	centre crack tension panel
ETM-MM	Engineering Treatment Model for Mismatched structures
CTOD	crack tip opening displacement
CMOD	crack mouth opening displacement
SENB	single-edge notched bend specimen

Differences in elastic material properties as well as in strain hardening exponents also play a role, however, in this paper we only focus on the problem of a mismatch in yield strengths.

Fig. 1 shows a family of load-Jintegral curves for SENB specimens with the same geometry but different mis-match levels in yield strength, Hao et al. (1995). From this diagram one sees that at low loads all curves coalesce. This is because under this initial loading the linear elastic field still dominates

the crack tip field, as assumed there is no mis-match in elasticity properties. With increasing load the curves diverge. This effect becomes very obvious in the fully plastic condition. From this diagram it is seen that the 'transition point' from the linear elastic stage to the fully plastic stage shifts its position, depending on the degree of mismatch, and under the same load level the variation in J-integral can be more than 1–100. Therefore one can conclude that the yield strength mis-match has a strong effect on the deformation behaviour in the elastic–plastic regime. The limit load, which symbolizes the above mentioned transition point, is a very important parameter for the crack driving force estimation in structures with mis-matched welded joints.

Efforts are being undertaken by various research groups to extend existing failure assessment procedures to heterogeneous structures, such as mismatched welded joints. This is of particular importance for undermatching cases, since as Fig. 1 shows, an assessment based on the assumption of homogeneous material ($M = 1$), may severely overestimate the load carrying capacity of a configuration with $M < 1$.

A joint French activity at Electricitée de France and Framatome is aimed at modifying the EPRI Handbook (Kumar et al., 1981), by creating yield load solutions for characteristic mismatch configurations which have then to be used in the EPRI handbook J formulas; the resulting procedure is referred to as the ARAMIS Method (Gilles and Franco, 1994). The yield loads are determined using slip-line theory.

The EPRI Handbook is also used by a research group at Edison Welding Institute and tailored to mismatch, Wang et al. (1996). The thus obtained J results are then used as input for a modified failure assessment diagram in the British document PD-6493 (British Standard Institution, 1991).

The R6 document (Milne et al., 1986), is being modified by Nuclear Electric. Limit loads have been derived for bend bars using slip-line theory (Joch et al., 1993; Burstow and Ainsworth, 1995). Furthermore, the relation between J and the CTOD has been discussed (Joch and Ainsworth, 1994).

A similar activity is being carried out in the authors' group. The Engineering Treatment Model (ETM) is a method for estimating the CTOD in terms of δ_5 and the J-integral as driving force parameters (Schwalbe, 1992). Its extension to heterogeneous structures — the ETM-MM — uses the

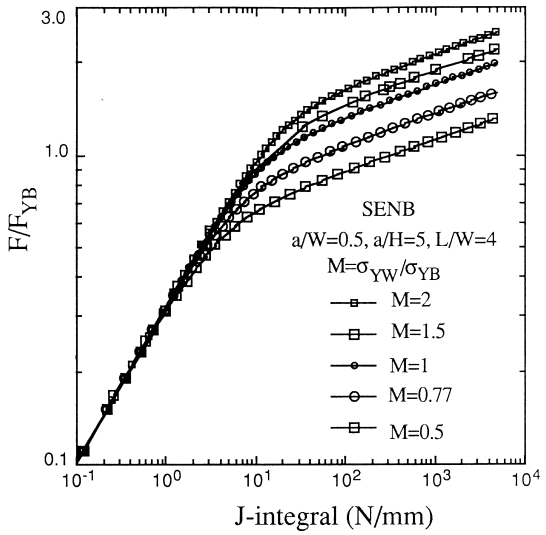

Fig. 1. Illustration of the effect of mismatching on the J-integral, finite element analysis (Hao et al., 1995).

basic ETM formulas with mismatch modified yield loads (Schwalbe et al., 1994; Hao et al., 1994a, 1994b, 1997). Up to now the center cracked tensile panel (CCT) has been treated, deriving yield loads for plane stress and plane strain (Hao et al., 1994b, 1997). The main tool is again the plane strain slip-line theory, amended by FE analyses including materials with strong strain hardening. Using FE analysis, some 3D studies have also been carried out (Hao et al., 1994a, 1994b).

In the present paper we will focus on the cracked bar under pure bending. In the homogeneous case the slip-line solution and corresponding expression of the yield load of notched bend bars have been derived by Hundy (1954) for a deep crack, and by Ewing and Hill (1967) for a shallow crack. Assuming that in mismatch specimens Hundy's slip-line field is available, the effect of the yield strength difference on the yield load and the relation between the J-integral and the CTOD for three point bending specimens has been discussed by Joch et al. (1993, 1994). Combining test results and numerical calculation (Reuter et al., 1994), have analyzed the constraint state and fracture behaviour of severely undermatched interleaf specimens ($M < 0.5$) with varying thickness under pure bending. They have found that when the ratio of weld metal height to remaining ligament length reaches 0.3 then there could be a transition from pop-in crack extension to stable crack growth. This means: a narrow undermatched weld layer can lead to a higher constraint state at the crack tip.

In the present work the main emphasis will be on extreme undermatching where the base material remains elastic. Solutions for plane strain and plane stress yield loads will be derived using slip-line theory. The case of moderate mismatch, where plastic deformation takes place both in weld metal and base plate will be treated as well. Finite element analysis will amend the slip-line work and provide some insight into 3D effects.

2. Idealizations

An actual welded joint is rather complicated, both metallurgically and geometrically, as depicted

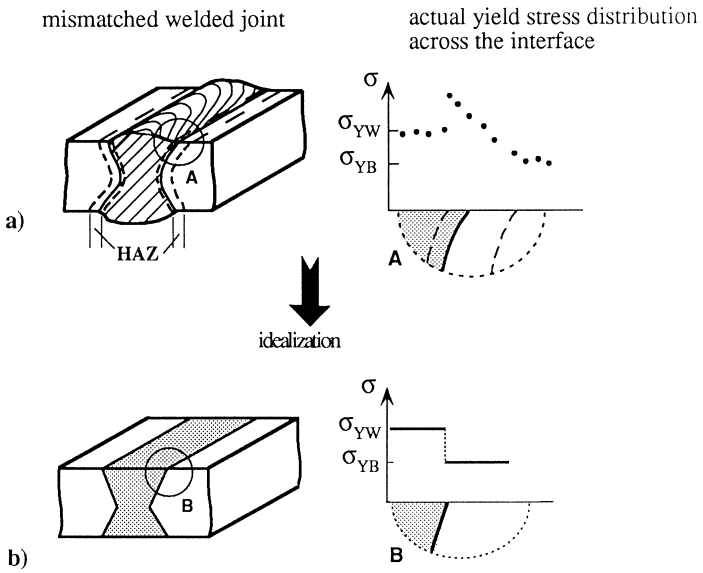

Fig. 2. The simplified model of a welded joint with heterogeneity.

schematically in Fig. 2(a). For simplification in the following analysis the effects of heat affected zones, residual stresses or other kinds of heterogeneity are omitted; the fusion line (see Fig. 2(a)) is modeled as an interface in a bi-material system as shown in Fig. 2(b). In this paper, the two models analyzed are shown in Fig. 3, in which the crack lies in the center line or the interface (fusion-line) of the welded joint. Both materials have the same elastic modulus and Poisson's ratio but the yield strength of the weld metal is lower or higher than that of the base material.

For the slip-line field analysis, the material is assumed to obey the law of elastic-perfect plasticity. Obviously, according to the difference in yield strength three possibilities exist: (i) plastic zone being confined to the soft weld metal layer (see Fig. 4(a)); (ii) penetrating both materials (see Fig. 4(b)) or (iii) most plastic deformation occurring in the base material (see Fig. 4(c)) when the yield strength of the weld metal is much higher than that of the base material. The first case is hereafter referred to as 'extreme undermatching' and will be treated in detail in the next section. The solutions for penetrating deformation field have also been derived in an approximate manner and will be presented afterwards. In 'case (iii)', the existence of a crack does not play any role in the ductile fracture behaviour as the plastic deformation takes place only in the base metal, so that it will not be discussed in this paper.

The models analysed are compiled in Fig. 3. They are characterized by two material parameters, σ_{YB} and σ_{YW}, and four geometrical parameters, a, W, H, and B, where B is the thickness of the model. In the present work, mainly the slip-line theory has been used for the analyses which allows to derive theortical solutions under plane strain and plane stress conditions. Such analytical expressions are convenient for engineering application. In addition, some finite element analyses have been performed to verify solutions and to obtain some results for 3D cases. As isoparametric elements may cause numerical problems in the fully plastic range (see Nagtegaal et al., 1974) the ABAQUS hybrid elements CPE8H and C3D20H, i.e. a quadratic displacement formulation with linear pressure, have been applied. A typical 3D mesh is shown in Fig. 17.

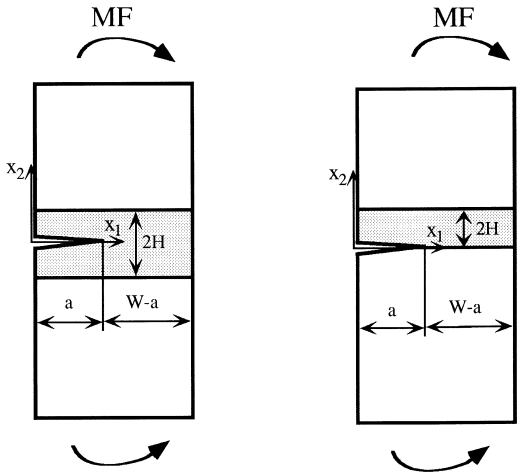

Fig. 3. The models analysed.

3. Extreme undermatching

3.1. The basic equations

Since in the case of extreme undermatching, all the plastic deformation is confined to the weld metal and the elastic strain is very small as compared to the plastic strain, it is reasonable to assume the following:

1. The base material is rigid.
2. The weld metal is rigid-perfectly plastic, obeying the von Mises yield criterion.

Thus, the slip-line field analysis of the general problems in Fig. 3(a) and (b) is simplified to the single-edge cracked finite width strips within the rotated rigid top and bottom boundaries, on which a pair of constant moments 'MF' is acting. It can mathematically be expressed as:

$$\text{at} \quad x_2 = \pm H: \quad \int_0^W x_1\sigma_{22}\,\mathrm{d}x_1 = \pm MF; \quad \int_0^W \sigma_{22}\,\mathrm{d}x_1 = \int_0^W \sigma_{12}\,\mathrm{d}x_1 = 0; \quad \sigma_{12} \le k_W \tag{2a}$$

$$\text{at} \quad x_2 = \pm 0 \quad \text{and} \quad 0 \le x_1 \le a: \quad \sigma_{22} = \sigma_{12} = 0$$

$$x_1 = 0 \quad \text{and} \quad x_1 = W: \quad \sigma_{11} = \sigma_{12} = 0 \tag{2b}$$

$$\text{Plane strain} \quad \varepsilon_{33} = \varepsilon_{13} = \varepsilon_{23} = 0$$

$$\text{Plane stress} \quad \sigma_{33} = \sigma_{13} = \sigma_{23} = 0 \tag{2c}$$

where σ_{ij} and ε_{ij} denote stress and strain components, respectively and, k_W is the shear yield stress of the weld metal.

In the present work the slip-line fields have been constructed for the middle and interfacially cracked layer with varying $(W-a)/H$ ratio. The corresponding expressions for yield load and the constraint parameter Q are deduced and listed in the following sections, where the parameter Q is defined by O'Dowd and Shih (1992) in the form

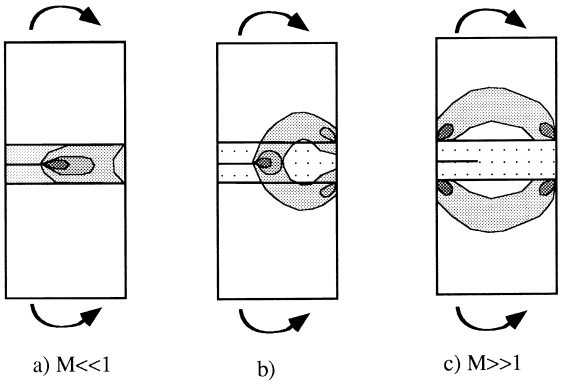

Fig. 4. Various deformation fields, depending on the mis-match level.

$$Q = \left.\frac{\sigma_{\varphi\varphi} - \sigma_{\varphi\varphi,\,\mathrm{HRR}}}{\sigma_{\mathrm{Y}}}\right|_{\varphi=0,\ \frac{r\sigma_{\mathrm{Y}}}{J}=2} \tag{3a}$$

for a material with strain hardening and

$$Q = \left.\frac{\sigma_{\varphi\varphi} - \sigma_{\varphi\varphi,\,\mathrm{Prandtl}}}{\sigma_{\mathrm{Y}}}\right|_{\varphi=0,\ \frac{r\sigma_{\mathrm{Y}}}{J}=2} \tag{3b}$$

for a material obeying the perfectly-plastic law; where φ is the angle in the polar coordinate system centered at the crack tip and the subscript Prandtl denotes the stress component calculated from the solution of the Prandtl crack tip field.

3.2. Middle crack in pure bending, plane strain condition

Obviously, under this condition the stress-strain distribution in the weld metal layer is determined by the layer geometry, i.e., the ratio of $(W-a)/H$ (Fig. 3(a)).

Case I: $((W-a)/H \leq 1.976)$**.** In this case mismatching does not play any role since the distance from the boundary of the base material to the crack tip is larger than the active plastic zone size under homogeneous conditions. Thus, the existence of the yield strength mismatch does not impose any extra constraint on the deformation field in the weld metal layer. From Hundy's field (see Hundy, 1954) for homogeneous pure bending (Fig. 5(a)), the stress distribution can be easily obtained using the traction-free boundary condition at the side AA′ in the compression zone ABCB′A′:

$$\sigma_{11} = 0, \quad \sigma_{22} = -2k_{\mathrm{W}}, \quad \sigma_{12} = 0, \quad \sigma_{\mathrm{m}} = -k_{\mathrm{W}} \tag{4a}$$

and on the slip arc OB:

$$\sigma_{\mathrm{m}} = k_{\mathrm{W}}[2\theta - 1]$$

$$\sigma_{11} = \sigma_{\mathrm{m}} + k_{\mathrm{W}}\cos 2\theta, \quad \sigma_{22} = \sigma_{\mathrm{m}} - k_{\mathrm{W}}\cos 2\theta, \quad \sigma_{12} = k_{\mathrm{W}}\sin 2\theta \tag{4b}$$

The corresponding yield load for unit thickness can be derived by integration along the arc OB and the straight line BA:

$$MF_{\mathrm{YM}} = \int_0^{\beta} k_{\mathrm{W}} r^2 \,\mathrm{d}\theta + k_{\mathrm{W}} l\sqrt{2}\left(r + \frac{l}{2}\right) \tag{4c}$$

where the constants r, l, and β are determined by the geometrical requirement below (refer to Fig. 6(a))

$$W - a - \frac{l}{\sqrt{2}} - r\left[\frac{1}{\sqrt{2}} + \sin\left(\beta - \frac{\pi}{4}\right)\right] = 0$$

and by the equilibrium conditions in the horizontal and vertical directions

$$\int_{\mathrm{OBA}} \sigma_{1i} n_i \,\mathrm{d}s = 0, \qquad \int_{\mathrm{OBA}} \sigma_{2i} n_i \,\mathrm{d}s = 0 \tag{5}$$

where n_i are the direction cosines of the vector which is normal to the infinitesimal small line segments on OBA.

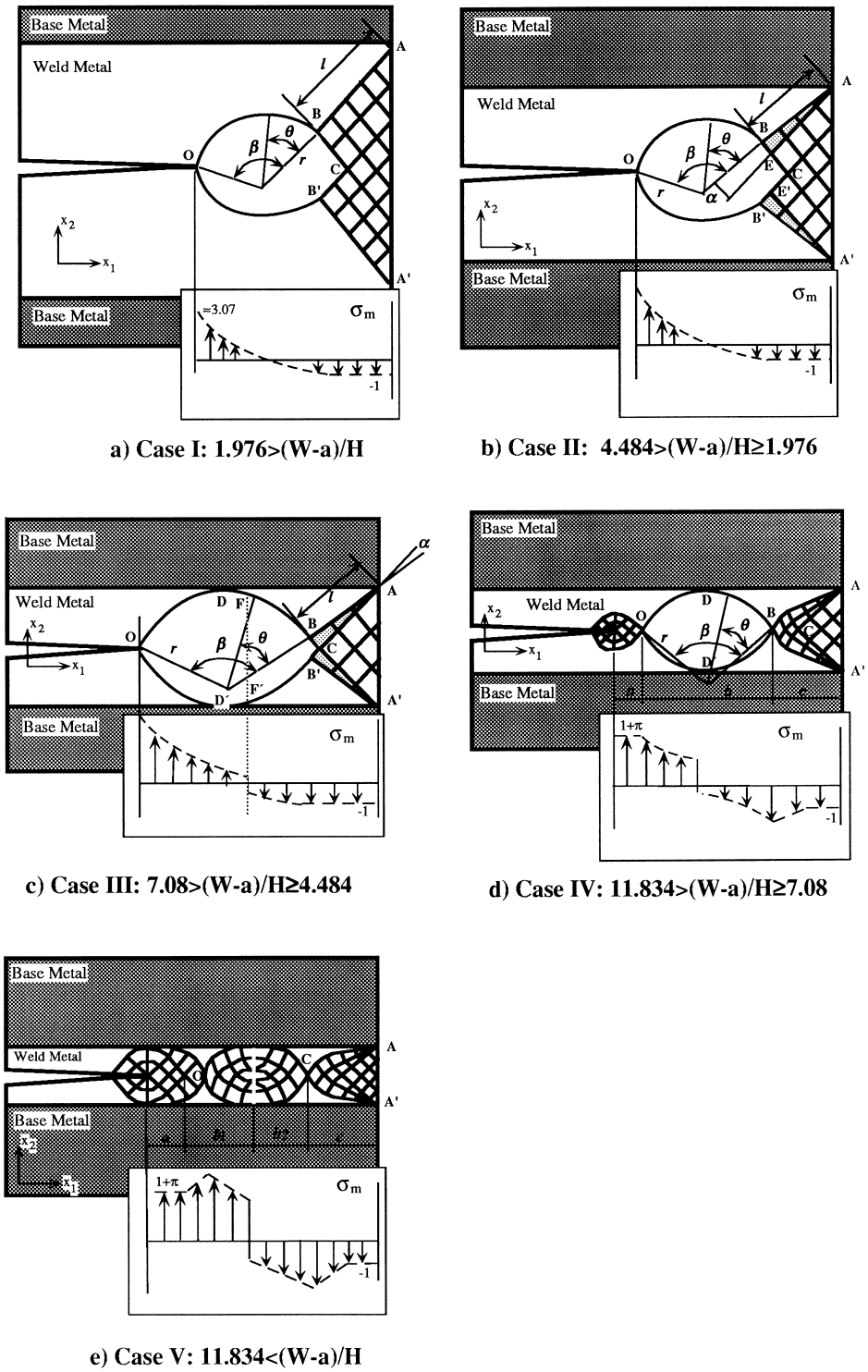

Fig. 5. The slip-line fields and corresponding distribution of the triaxial stress on the ligament for extreme undermatching, single edge cracked specimen (SENB) under pure bending.

The result of Eq. (4c) is then

$$MF_{\mathrm{YM}} = 0.6309\frac{\sigma_{\mathrm{YW}}(W-a)^2}{\sqrt{3}} \tag{6}$$

However, from the stress state (see Eqs. (4a) and (4b)) as well as the stress distributions for the cases shown in Fig. 5(b) and (c), we cannot determine the parameter Q at the crack tip directly, as in these cases the slip-line field solution for the bending configuration can only give the stress components along the slip-lines which radiate from the crack tip and which are inclined to the horizontal line with an angle larger than 45°. From this kind of slip-line fields the stress field surrounding the crack tip is not uniquely obtainable. In Fig. 6 two possible stress distributions are illustrated. In this figure we assume, asymptotically, that a small piece of straight slip-line O′O (or O′O″) exists. It radiates from the crack tip and is connected to the arc OB in the global slip-line field as shown in Fig. 6. Thus, the stress components on these small lines are constant and equal to the components at the point O on the arc OB in Fig. 6, for example, using Eq. (4b). From Fig. 6 one sees that the plastic deformation may expand from the line O′O (or O′O″) ahead of the crack tip and form a diamond-like plastic zone O′HFH′ like that in Prandtl field (Fig. 6(a)), or be confined to a small fan-like field with the material in the area just ahead of the crack tip staying in the elastic state (Fig. 6(b)).

Hereafter we use the subscript O′O″ to denote the quantities on O′O (or O′O″). For the case in Fig. 6(a) the stresses in the diamond-like zone O′HFH′ can be calculated by slip-line theory as shown by O'Dowd and Shih (1992). They are given as follows:

$$\sigma_{\mathrm{m}} = \sigma_{\mathrm{m,\,O'O}} + 2k_{\mathrm{W}}\theta_{\mathrm{HO'O}}$$

$$\sigma_{11} = \sigma_{\mathrm{m}} - k_{\mathrm{W}}, \quad \sigma_{22} = \sigma_{\mathrm{m}} + k_{\mathrm{W}}, \quad \sigma_{12} = 0$$

where $\theta_{\mathrm{HO'O}}$ represents the angle between the lines O′H and O′O.

Thus, according to the definition in (4b), in this case the constraint at the crack tip is

$$Q_{\mathrm{upper}} = \frac{\sigma_{\mathrm{m,\,O'O}} + k_{\mathrm{W}}(2\theta_{\mathrm{HO'O}} - \pi - 1)}{\sigma_{\mathrm{YW}}} \tag{7}$$

where the subscript 'upper' means that the relation (6) is an 'upper bound estimate' for the constraint state because of presuming the plastic zone O′HFH′.

For the case in Fig. 6(b), in the fan O′HH′ material points remain elastic. A boundary-value problem has been formulated as follows:

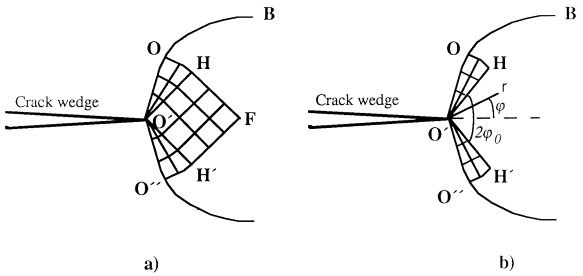

Fig. 6. Illustration of the asymptotic slip-line field ahead of a crack tip of a bending specimen: (a) upper-bound solution; (b) lower-bound solution.

$$\Delta\Delta\Phi(r,\vartheta)=0 \tag{8a}$$

$$\sigma_{\vartheta\vartheta}|_{\vartheta=\pm\varphi_0}=\sigma_{\mathrm{m,\,OH}},\quad \sigma_{r\vartheta}|_{\vartheta=\pm\varphi_0}=\pm k_{\mathrm{W}} \tag{8b}$$

where Φ is Airy's stress function:

$$\sigma_{\vartheta\vartheta}=\frac{\partial^2\Phi}{\partial r^2},\quad \sigma_{rr}=\frac{\partial\Phi}{r\partial r}+\frac{\partial^2\Phi}{r^2\partial\vartheta^2},\quad \sigma_{r\vartheta}=-\frac{\partial}{\partial r}\left(\frac{\partial\Phi}{r\partial\vartheta}\right)$$

Using the general theory of elasticity (see Timoshenko and Goodier, 1970), it is not difficult to determine the dominating term of Φ according to the boundary condition (8b). After having investigated several examples for the solutions of Eq. (8a) we find that we can simply use the expression

$$Q_{\mathrm{lower}}=\frac{\sigma_{\mathrm{m,\,O'O}}-k_w(\pi+1)}{\sigma_{\mathrm{YW}}} \tag{9}$$

as the 'lower bound estimate' of the constraint state for the bending configuration.

The asymptotic fields in Fig. 6 and the resulting relations (7) and (9) are generally applicable to the bending configuration with any ratio of $(W-a)/H$. Thus, from the slip-line field in Fig. 5(a) one can determine $\sigma_{\mathrm{m,\,O'O}}$, so that from Eqs. (7) and (9) one obtains

$$Q_{\mathrm{upper}}=-0.01745;\qquad Q_{\mathrm{lower}}=-0.4538 \tag{10}$$

Case II: $(1.976<(W-a)/H\leq 4.484)$**.** In Fig. 5(b) the global kinematically available deformation field, (i.e., the arc slip-line connecting the crack tip to the compression zone) is similar to the field in Fig. 5(a). However, the size of the compressive plastic zone is reduced because of the limited height of the weld metal, although a fan-shaped field centered at the interface edge emerges (denoted as ABE in Fig. 5(b)), accompanied by an increased compressive stress, whereas a slightly increased stress appears at the crack tip and the global yield load is also elevated. This stress state can be expressed as follows in the compression zone AECE′A′:

$$\sigma_{11}=0,\quad \sigma_{22}=-2k_{\mathrm{W}},\quad \sigma_{12}=0,\quad \sigma_{\mathrm{m}}=-k_{\mathrm{W}} \tag{11a}$$

on the slip arc EB

$$\sigma_{\mathrm{m}}=k_{\mathrm{W}}[2\theta'-1]$$

$$\sigma_{11}=\sigma_{\mathrm{m}}+k_{\mathrm{W}}\cos 2\theta',\quad \sigma_{22}=\sigma_{\mathrm{m}}-k_{\mathrm{W}}\cos 2\theta',\quad \sigma_{12}=k_{\mathrm{W}}\sin 2\theta' \tag{11b}$$

where θ' indicates the position of the material point on the slip line arc EB; at the point, E $\theta'=0$ and at the point B, $\theta'=\alpha$.

On the arc OB

$$\sigma_{\mathrm{m}}=k_{\mathrm{W}}(2\theta+2\alpha-1)$$

$$\sigma_{11}=\sigma_{\mathrm{m}}+k_{\mathrm{W}}\cos 2(\theta+\alpha),\quad \sigma_{22}=\sigma_{\mathrm{m}}-k_{\mathrm{W}}\cos 2(\theta+\alpha),\quad \sigma_{12}=k_{\mathrm{W}}\sin 2(\theta+\alpha) \tag{11c}$$

The global yield load of the slip-line field in Fig. 5(b) can be calculated using

$$MF_{YM} = \int_0^{\beta} k_W r^2 \, d\theta + [2\alpha - 1] k_W l \left(r + \frac{l}{2} \right) \tag{11d}$$

For the slip-line field in Fig. 5(b), there are four unknown variables: r, l, α and β. They are determined by using the equilibrium condition, Eq. (5), and the following geometric requirements:

$$W - a - l\cos\left(\frac{\pi}{4} - \alpha\right) - r\left[\cos\left(\frac{\pi}{4} - \alpha\right) + \cos\left(\alpha + \beta - \frac{\pi}{4}\right)\right] = 0 \tag{11e}$$

and

$$H - l\sin\left(\frac{\pi}{4} - \alpha\right) - r\left[\sin\left(\frac{\pi}{4} - \alpha\right) - \sin\left(\alpha + \beta - \frac{\pi}{4}\right)\right] = 0 \tag{11f}$$

For varying $(W - a)/H$ the integral (11d) has been solved and the results are fitted by the following polynomial:

$$MF_{YM} = \frac{\sigma_{YW}(W - a)^2}{\sqrt{3}}\left[0.6315 - 0.01059\psi + 0.0049\psi^2\right] \tag{12a}$$

where

$$\psi = \frac{W - a}{H}$$

and the upper and lower constraint parameter Q at the crack tip is given as:

$$Q_{upper} = 0.9745 - 1.13665\psi + 0.3123\psi^2 \quad \text{for } 0.506 \leq \frac{1}{\psi} < 0.4424$$

$$Q_{upper} = 0 \quad \text{for } 0.4424 \leq \frac{1}{\psi} < 0.223 \tag{12b}$$

and

$$Q_{lower} = -0.6373 + 0.1257\psi - 0.016175\psi^2 \tag{12c}$$

Case III: $(4.484 < (W - a)/H \leq 7.08)$**.** When the value of $(W - a)/H$ reaches 4.484, the top of the rotation arc will touch the interface between the weld and the base metal BC at the point D in Fig. 5(c). This hinders the fact that a stronger constraint provided by the base metal takes place which confines the slip-line field in weld metal with a large rotation angle β. A stress jump will emerge at the point F (or F′) to maintain the rotation along the arc OB and keep the global equilibrium. This jump is similar to a 'plastic hinge' for a plastic beam under bending in the homogeneous case: the material points on the line connecting point F and F′ in Fig. 5(c) are in an elastic condition because on the left side of the point F (or F′) tension dominates whereas on the right side compression dominates. According to the stress distributions introduced in the following, the unknown variables in Fig. 5(c): r, l, α, β, and the position of the point F as well as the value of the stress discontinuity, are determined by the global equilibrium condition (5), the geometrical requirements, Eqs. (11e) and (11f), and the following condition:

$$\beta - \alpha \geq \frac{\pi}{2} \tag{13a}$$

When $(W-a)/H = 7.08$, the stress jump reaches a maximum value ($\Delta\sigma_{22} = 4k_W$) and the point F coincides with the point D. From the slip-line field in Fig. 5(c), we obtain the stress distribution on the ligament in the compression zone ACA′ as follows:

$$\sigma_{11} = 0, \quad \sigma_{22} = -2k_W, \quad \sigma_{12} = 0, \quad \sigma_m = -k_W \tag{13b}$$

On the arcs CB and BF the stress distribution can be expressed by Eqs. (11b) and (11c)).

Assuming that at the point F there is a jump of σ_m, i.e., $\Delta\sigma_m$; then the stresses on the arc ODF are:

$$\sigma_m = k_W(2\theta + 2\alpha - 1) + \Delta\sigma_m$$

$$\sigma_{11} = \sigma_m + k_W\cos 2(\theta + \alpha), \quad \sigma_{22} = \sigma_m - k_W\cos 2(\theta + \alpha), \quad \sigma_{12} = k_W\sin 2(\theta + \alpha) \tag{13c}$$

In comparison with the case in Fig. 5(b), an additional variable appears, which is resolved by using Eq. (16a) within an equality sign.

The corresponding yield load has been derived by Eqs. (11b)–(11d), 13(b) and (13c) and it is fitted by a polynomial of the form:

$$MF_{YM} = \frac{\sigma_{YW}(W-a)^2}{\sqrt{3}}\left[0.4445 + 0.0616\psi - 0.00176\psi^2\right] \tag{14a}$$

and the constraint parameter Q at the crack tip has a value between:

$$Q_{lower} = 0.01 - 0.30846\psi + 0.04339\psi^2 \quad \text{and} \quad Q_{upper} = 0 \tag{14b}$$

Checking this relation one may find that when $(W-a)/H$ approaches 7.08 the value of Q_{lower} vanishes so that $Q_{lower} = Q_{upper}$. Under this condition the high constraint provided by the rigid base material confines the formation of a unique Prandtl field to the crack tip.

Case IV: ($7.08 < (W-a)/H \leq 11.834$)**.** In this case a Prandtl field has already formed at the crack tip and the stress level in this area cannot be changed any more. Increasing the ratio of $(W-a)/H$ will result in increasing size of the Prandtl field around the crack tip, until $(W-a)/H = 11.834$ when the top of the Prandtl field touches the interface between the weld and the base metals. The slip-line field has been constructed as shown in Fig. 5(d). The slip-line field PABA′C has already been given in the case of CCT in Appendix 1 of Hao et al. (1997). The stress distribution in the Prandtl field is well known; at the point O it gives

$$\sigma_{11}|_O = \pi k_W, \quad \sigma_{22}|_O = (2+\pi)k_W, \quad \sigma_m|_O = (1+\pi)k_W \tag{15a}$$

On the arc OD:

$$\sigma_m = \sigma_m|_O - 2k_W(\beta - \theta)$$

$$\sigma_{11} = \sigma_m + k_W\cos 2\theta, \quad \sigma_{22} = \sigma_m - k_W\cos 2\theta, \quad \sigma_{12} = k_W\sin 2\theta \tag{15b}$$

On the arc DB:

$$\sigma_m = \sigma_m|_O - 2k_W(2 + \beta - \theta)$$

$$\sigma_{11} = \sigma_m + k_W \cos 2\theta, \quad \sigma_{22} = \sigma_m - k_W \cos 2\theta, \quad \sigma_{12} = k_W \sin 2\theta \tag{15c}$$

The corresponding yield load has been calculated by integrating the stress along the slip-lines on the ligament and the result is fitted by the polynomial:

$$MF_{YM} = \frac{\sigma_{YW}(W-a)^2}{\sqrt{3}}\left[0.5837 + 0.0299\psi\right] \tag{16a}$$

Because in this stage a Prandtl field exists at the crack tip

$$Q = 0 \tag{16b}$$

Case V: $((W-a)/H > 11.834)$**.** When the size of the Prandtl field equals half the height of the weld metal layer, the state of stress distribution around the crack tip is fixed regardless of how large the ratio $(W-a)/H$! In addition to the high stress value at the crack tip, a second stress peak ahead of the front of Prandtl field appears because of the severe constraint on the ligament. The value of this stress peak and its distance from the crack tip increases with increasing $(W-a)/H$. On the right side of the stress discontinuity line (the plastic hinge) the deformation condition is similar to the case of 'the compression of a perfectly plastic block between rough rigid plates' introduced by Hill (1951) and Prandtl (1923) and on the left side it is similar to the case of 'extremely undermatched CCT under tension' which has been shown by Hao et al. (1997). In both cases the slip-lines can be described by two orthogonal cycloid families. The slip-line field is shown in Fig. 5(e), for which the stress field has been given by Hao et al. (1997), Hill (1951) and Prandtl (1923) and the corresponding yield load can be easily obtained. It is fitted by the polynomial:

$$MF_{YM} = \frac{\sigma_{YW}(W-a)^2}{\sqrt{3}}\left[0.5676 + 0.03115\psi\right] \tag{17a}$$

with the constraint at the crack tip:

$$Q = 0 \tag{17b}$$

Using slip-line theory, expressions for yield load and constraint have been derived for the whole range of $(W-a)/H$ values. Corresponding finite element modeling has also been performed. Fig. 7(a) compares the limit moment determined using Eqs. (6), (12a), (14a), (16a) and (17a) with that determined by finite element calculations. Fig. 7(b) shows the constraint and its dependence on the weld metal geometry, determined by the slip-line solutions for bending and tension configurations and compared with the finite element calculations. Fig. 8 illustrates the stress distribution for the case $H/(W-a) = 12.5$, obtained using the slip-line solution and finite element modeling. On this diagram one clearly sees the stress jumping at the 'plastic hinge' and the two stress peaks at about the middle position on both the tension and compression sides.

4. Slight undermatching and overmatching

4.1. Central crack, plane strain condition

The solutions discussed in the previous section have been derived under the assumption that the base

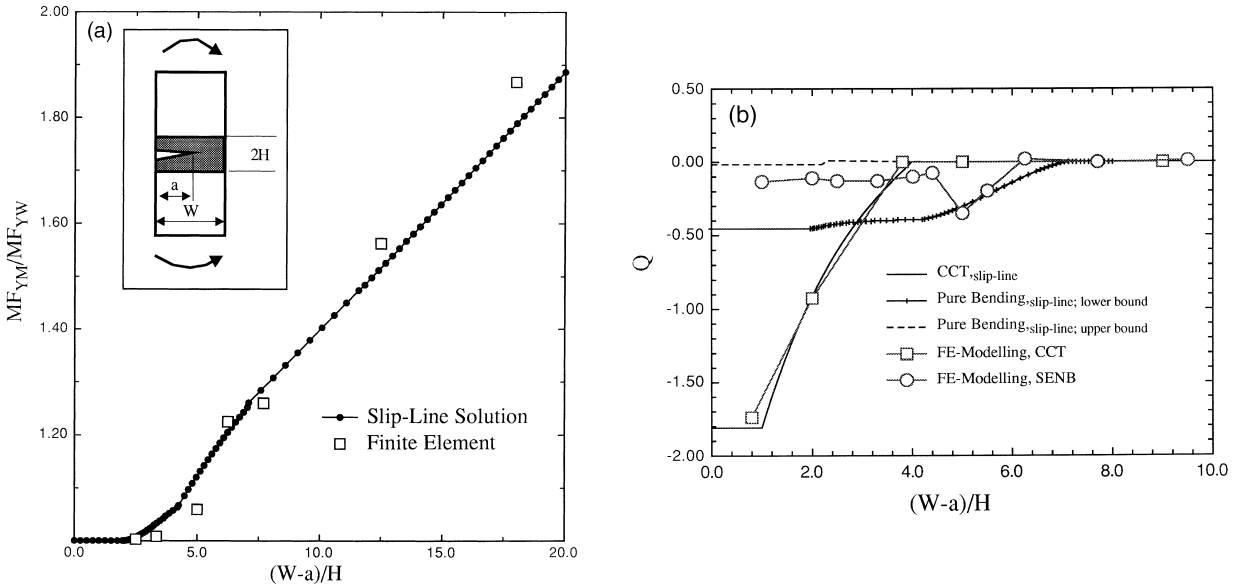

Fig. 7. (a) Comparison of the yield load derived from the slip-line solutions and finite element analysis for extreme undermatching. (b) Constraint and its dependence on geometry, the CCT data were taken from Schwalbe et al. (1994).

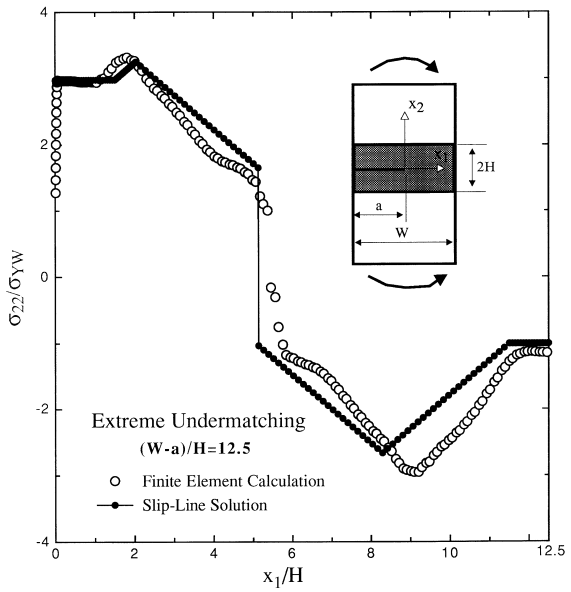

Fig. 8. Stress distribution ahead of the crack tip on the ligament ($x_2 = 0$) for the case of Fig. 5(e), slip-line solution and finite element calculation.

material is rigid or deforms only elastically so that the plastic deformation is always confined to the weld metal, this represents extreme undermatching. If the base material deforms plastically but the mismatch in yield stress, expressed by the factor $M = (\sigma_{YW}/\sigma_{YB})$ is still much smaller than unity, the extreme undermatching condition can also hold so that the slip-line solutions obtained previously are still applicable. However, if the ratio M is close to, but still less than unity, undermatching is still present and plastic deformation may extend from the weld strip into the base material. This is because the base metal is not strong enough to remain in the elastic state and to maintain the high constraint as in the case for extreme undermatching. If the ratio M is greater than unity, in other words, for overmatching condition, the plastic zone will penetrate both metals.

According to the degree of mismatch and the value of the ratio $H/(W-a)$ the plastic deformation may begin at the crack tip and penetrate both metals or take place merely in the base metal when M is large, as illustrated in Fig. 4(b) and (c). Only the former will be taken into account in the present work.

As mentioned above, for a mismatched joint in bending the 'assumed slip-line field' as shown in Fig. 9(a), which is similar to the homogeneous case, has been introduced and the relationship between the J-integral and the CTOD has been investigated by Joch et al. (1993, 1994) and Burstow and Ainsworth (1995). It has been reported that for a large range of $(W-a)/H$ values and mismatching degrees the solutions based on the slip-line field in Fig. 9(a) provide satisfactory estimates for application.

However, it is well known that the classical slip line theory is derived for homogenous perfectly-plastic material (see Refs. Prandtl, 1923; Hill 1951). In the case of slip-lines penetrating an interface in a bi-materials system (e.g. Fig. 3), additional conditions and requirements are necessary. According to the discussion in Appendix A, in the present work two kinds of slip-line fields for bending have been constructed, Fig. 9(b) and (c). For the slight mismatching condition, the field in Fig. 9(b) is presented. The slip-lines radiate from the crack tip and penetrate both materials. However, due to the traction-free boundary condition on the side AA′ the slip-line has to intersect the line AA′ below 45°. Thus, a

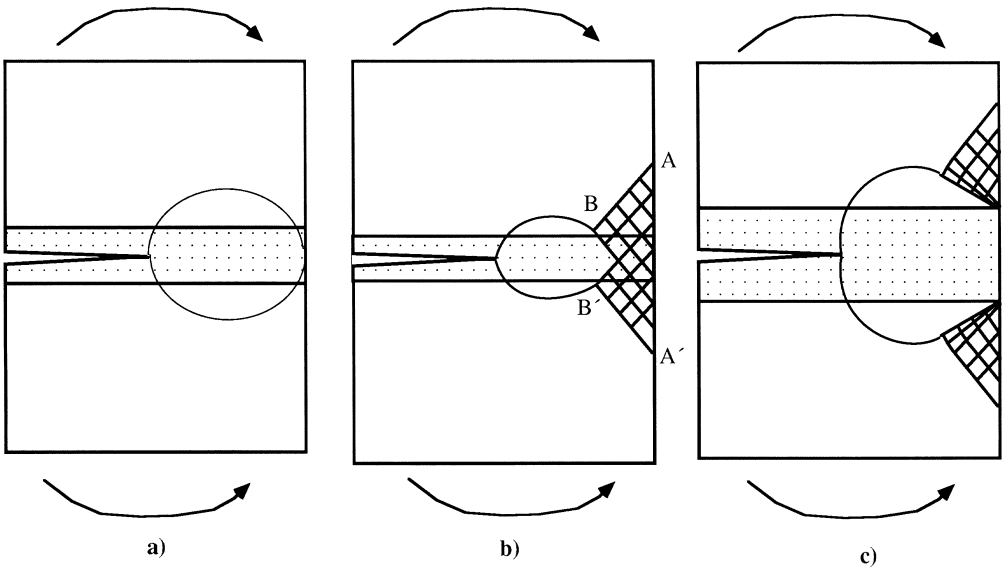

Fig. 9. (a) The 'assumed' slip-line field suggested by Joch et al. (1993, 1994). (b) The slip-line field for slight mismatching. (c) The slip-line field for strong overmatching.

constant compressive stress zone ABB′A′ appears on the ligament away from the crack tip. With increasing overmatching, deformation along the slip-line field shown in Fig. 9(c) will dominate, because in the weaker base metal plastic deformation becomes more favorable. In this case the interface edge is a singularity point of stress and strain. In engineering application crack initiation and growth could occur at this point, instead of the crack tip, as the latter is surrounded by the harder weld metal. When M is higher than a certain value, plastic strain will be suppressed in the weld metal. In this case the deformation field shown in Fig. 4(c) is present. To verify the slip-line fields constructed in Fig. 9(b) and (c), the equivalent plastic strain contours obtained by finite element analysis are shown in Fig. 10. Fig. 11(b) shows the yield load as determined from the slip-line solutions together with some finite element results.

Similar to the analysis by Hao et al. (1997), we define the yield load ratio R:

$$R = \frac{MF_{\text{YM, penetrating slip-line}}}{MF_{\text{YM, weld strip slip-line}}} \tag{18}$$

For $R < 1$ the penetrating slip-line solution, i.e. the solution given in Fig. 9(b), is relevant whereas for $R > 1$ the slip-line confined in the weld strip is valid, see Hao et al. (1997), Fig. 12. Based on the slip-line analysis and numerical calculation, the parameter R can be expressed approximately in the form as:

$$R = \frac{MF_{\text{YB}} \cdot f(\varphi, M)}{MF_{\text{YM, weld strip slip-line}}}; \quad \varphi \leq 1 \tag{19}$$

where $MF_{\text{YM, weld strip slip-line}}$ is determined by Eqs. (6), (12a), (14a), (16a) and (17a); and

$$f(\varphi, M) \approx 1 - M\varphi(M-1)(\varphi - 1), \quad \varphi = 1.976\frac{H}{W-a} \tag{20}$$

4.2. Extreme undermatching: interface crack, plane strain condition

Without great alteration of the results obtained previously we may derive the slip-line fields for the case that the crack is located on the fusion line (interface crack). Because of the limited space we consider only the condition of extreme undermatching with a large $(W-a)/H$ ratio ($(W-a)/H > 11.5$). The slip-line field is shown in Fig. 12(a). Fig. 12(b) displays the contour of equivalent plastic strains from the finite element calculation, demonstrating good agreement of both approaches. The corresponding yield load can be expressed by a polynomial of the form:

$$MF_{\text{YM}} = \frac{\sigma_{\text{YW}}(W-a)^2}{\sqrt{3}}(0.58091 + 0.0321644\psi) \quad \text{for } \psi > 11.5 \tag{21}$$

In this case the maximum principal stress at the crack tip front is

$$\sigma_{\varphi\varphi} = \frac{\sigma_{\text{YW}}(1 + 1.5\pi)}{\sqrt{3}} \tag{22a}$$

If we assume that the definition of constraint state in (4b) is still applicable for an interface crack, then Eq. (22a) can be substituted into (4b) to obtain Q:

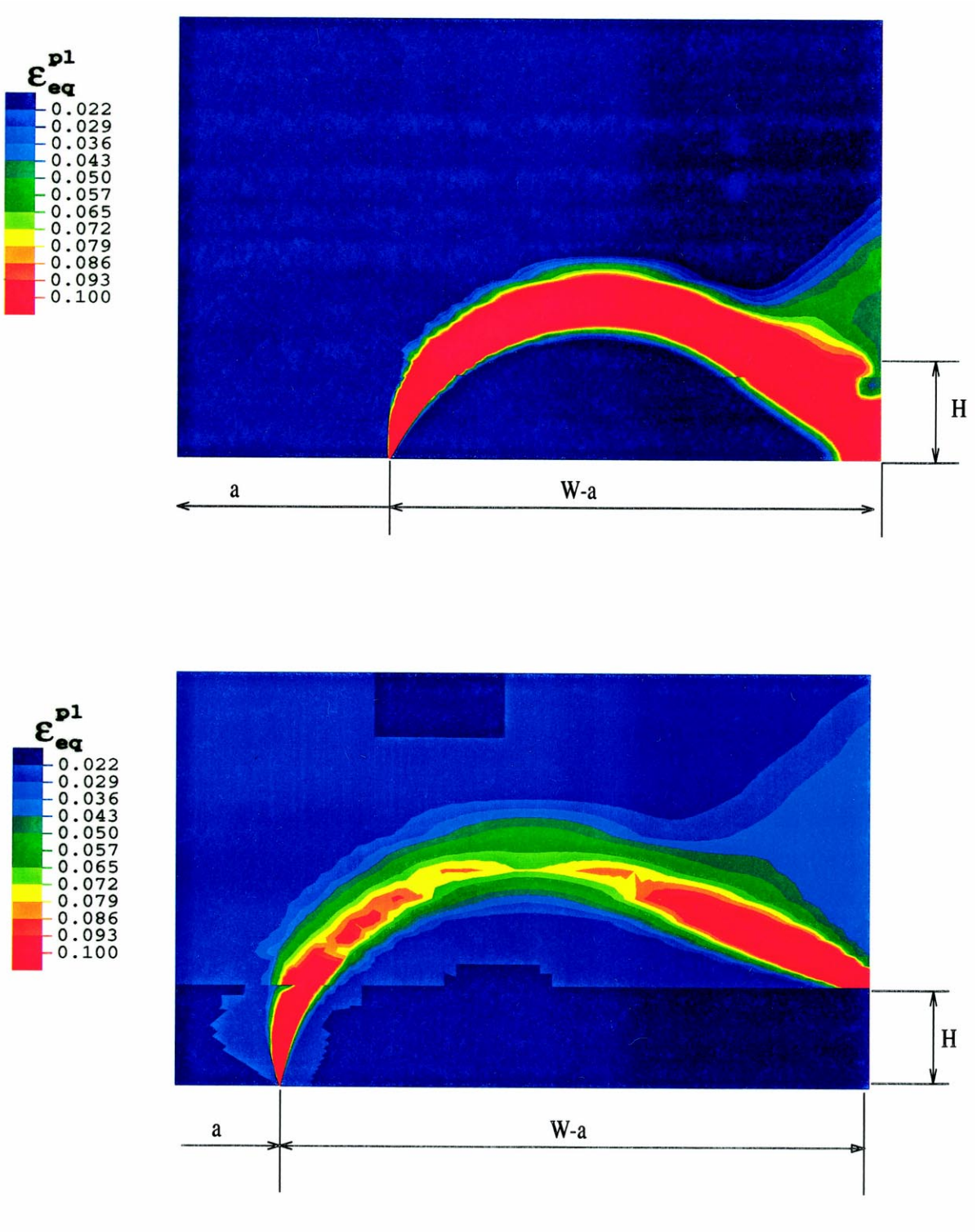

Fig. 10. Finite element modeling for the cases in Fig. 9(b) and (c).

$$Q = \frac{\sqrt{3}(\pi/2 - 1)}{4} = 0.22 \tag{22b}$$

4.3. Extreme undermatching: central crack, plane stress solution

The slip-line solution is illustrated in Fig. 13, which has been constructed using Hutchinson's solution (Hutchinson, 1968) at the crack tip connected to the field ABCDO on the ligament. In-between there is a stress jump. The stress distribution can be described by

in AOB

$$\sigma_r = \frac{\sigma_{YW}}{2}(\cos 2\theta - 1); \quad \sigma_\theta = -\frac{\sigma_{YW}}{2}(1 + \cos 2\theta); \quad \sigma_{r\theta} = -\frac{\sigma_{YW}}{2}\sin 2\theta \tag{23a}$$

in BOC

$$\sigma_r = \frac{\sigma_{YW}}{4}\left[(1 - \cos 2\theta_{AOB})\cos 2(\theta - \theta_{AOB}) - 3\cos 2\theta_{AOB} - 1 - 2\sin 2\theta_{AOB}\sin 2(\theta - \theta_{AOB})\right]$$

$$\sigma_\theta = -\frac{\sigma_{YW}}{2}(1 + 3\cos 2\theta_{AOB}) - \sigma_r;$$

$$\sigma_{r\theta} = \frac{\sigma_{YW}}{2}\left[(\cos 2\theta_{AOB} - 1)\sin 2(\theta - \theta_{AOB}) - 2\sin 2\theta_{AOB}\cos 2(\theta - \theta_{AOB})\right] \tag{23b}$$

and

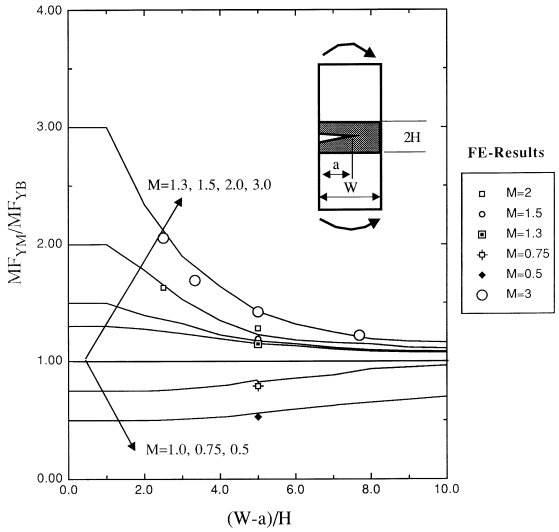

Fig. 11. Yield load obtained from the slip-line solutions for under and overmatching, plane strain, normalized with the yield load of a homogeneous specimen made of base material; and comparison with some FE results.

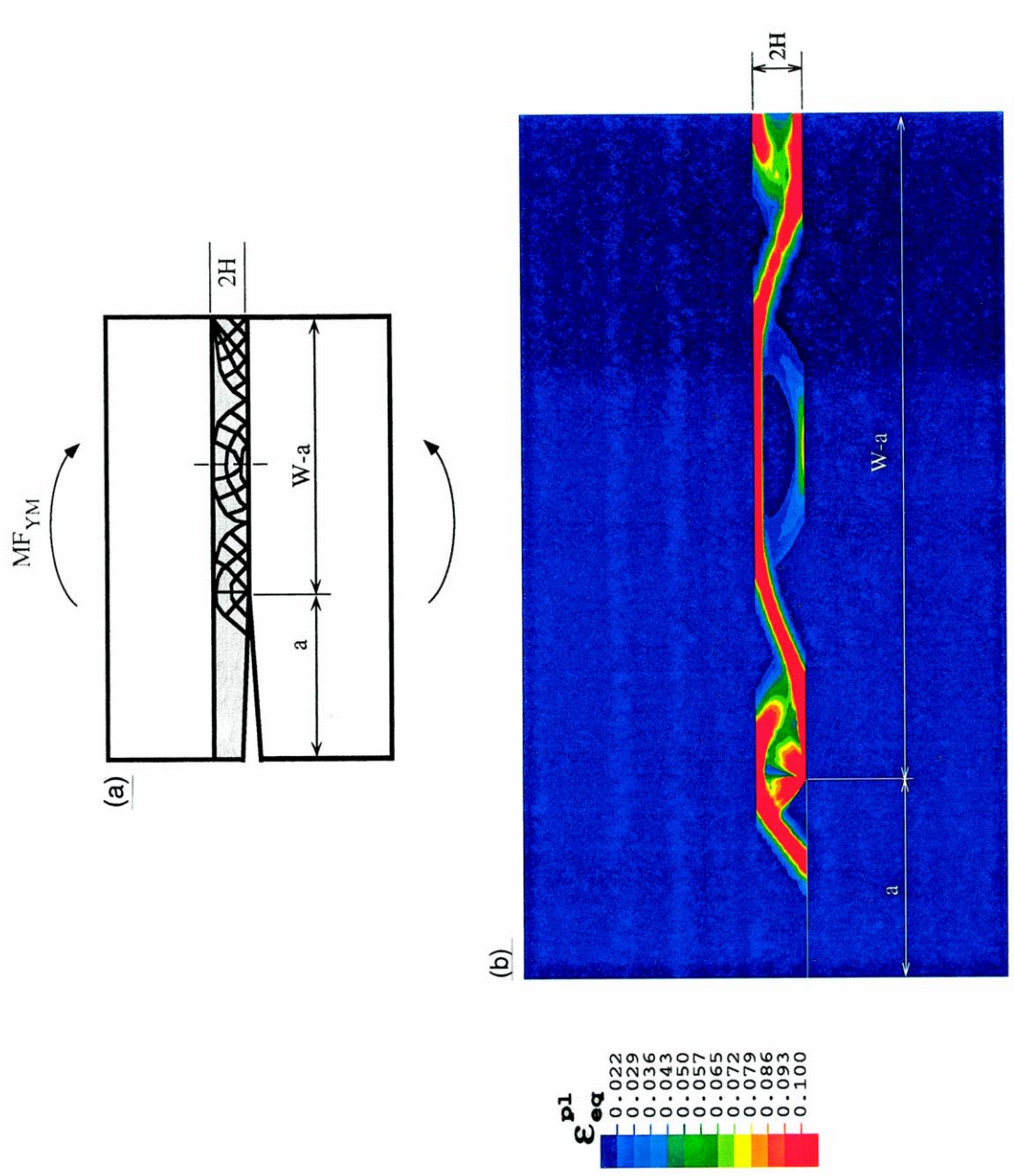

Fig. 12. (a) The slip-line field for an interface crack, extreme undermatching, $(W-a)/H > 12$. (b) Finite element verification of the slip-line field in Fig. 12(a).

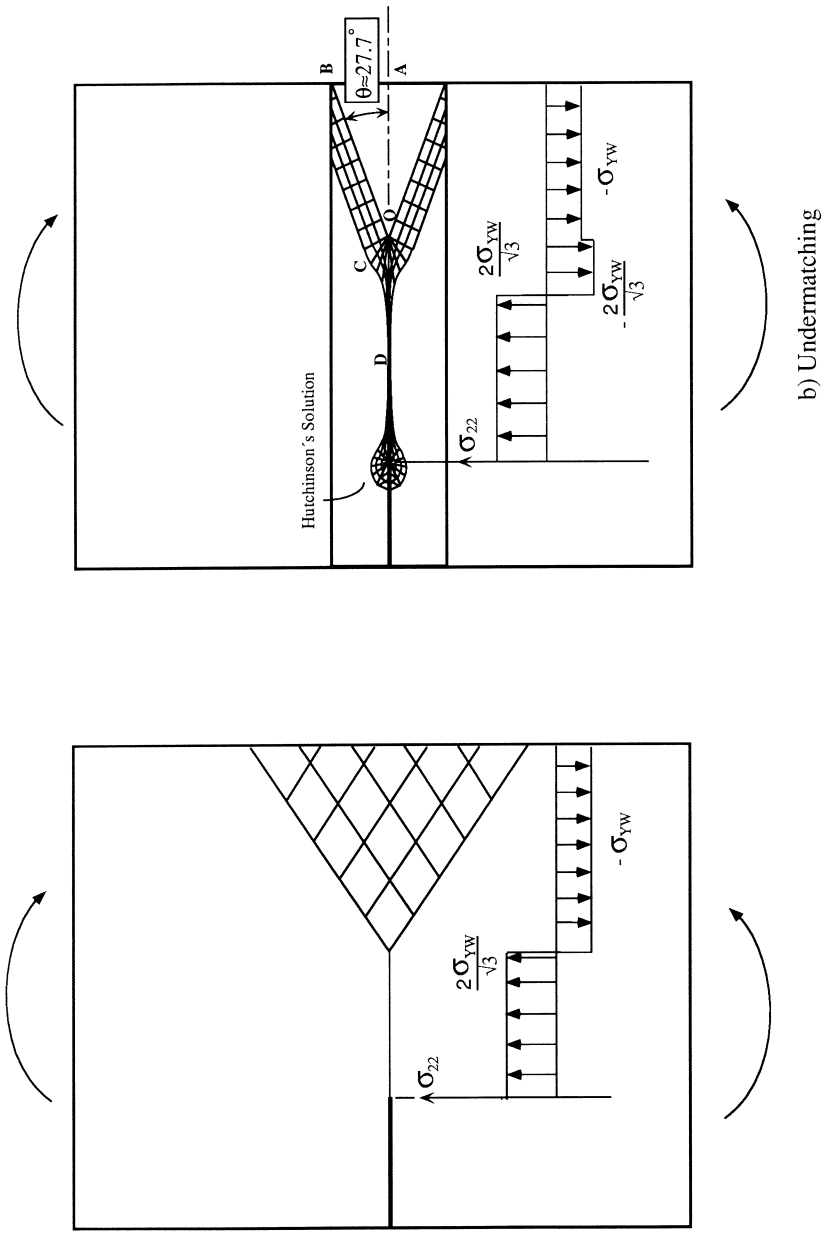

Fig. 13. Slip-line field for plane stress bend specimens.

$$\theta_{AOB} = 27.78^\circ \tag{23c}$$

in COD

$$\sigma_r = \frac{\sigma_{YW}}{2\sqrt{3}}\cos\theta, \quad \sigma_\theta = \frac{\sigma_{YW}}{\sqrt{3}}\cos\theta; \quad \sigma_{r\theta} = \frac{\sigma_{YW}}{\sqrt{3}}\sin\theta \tag{23d}$$

From this solution the yield load is

$$MF_{YM} = \frac{2\sigma_{YW}}{\sqrt{3}}\left[x_1^2 + x_2^2 + \frac{1.89\sqrt{3}}{2}H(x_2 + 0.945H)\right] \quad \text{for } \frac{W-a}{H} > 1.89 \tag{24}$$

where

$$x_1 = \frac{W - a - 0.2532H}{2}; \qquad x_2 = \frac{W - a - 1.8661H}{2}$$

5. The effect of thickness

When an actual bend specimen with finite thickness is considered, the question of how to determine its yield load arises.

For the cases of slight undermatching and overmatching, the global slip-line fields as shown in Fig. 9(b) and (c) are similar to the homogeneous case shown in Fig. 5(a). Because thickness effects in homogeneous specimens are well understood, in this section we focus on the 3D bending configuration within an extremely undermatched welded joint.

A 3D finite element analyses for specimens with seven thicknesses, ranging from $B/W = 0.02$ to 1, have been performed. Three results are shown in Fig. 14, from which one finds that the shape of the plastic zone at the middle section of specimens is similar to that derived by the slip-line field in 2D condition. For example, in the thinnest specimen the plastic zone is close to that indicated in Fig. 13 under plane stress condition. In the thickest specimen it has the same type as given in Fig. 5(e), an obvious Prandtl field can be observed in the middle section near the crack tip. Clearly, for this specimen the thickness is large enough to maintain plane strain condition in its middle section.

Numerical fitting has been used to the data calculated for the seven thicknesses. The yield load of extremely undermatched bend specimens can be expressed by the polynomial expression:

$$\text{if} \quad B \ll \left[\frac{K_I}{\sigma_{YW}}\right]^2, \quad 4 < \frac{W-a}{H}$$

for the case $B/H < 20$

$$MF_{YM} = MF_{YM,\ \text{plane stress}}\left\{1 + \Delta MF_{YM} f\left(\frac{B}{H}\right)\right\} \tag{25a}$$

where

$$f\left(\frac{B}{H}\right) = -0.0183 + 0.083\left(\frac{B}{H}\right) + 0.0054\left(\frac{B}{H}\right)^2 - 0.0007\left(\frac{B}{H}\right)^3 + 0.0000168\left(\frac{B}{H}\right)^4$$

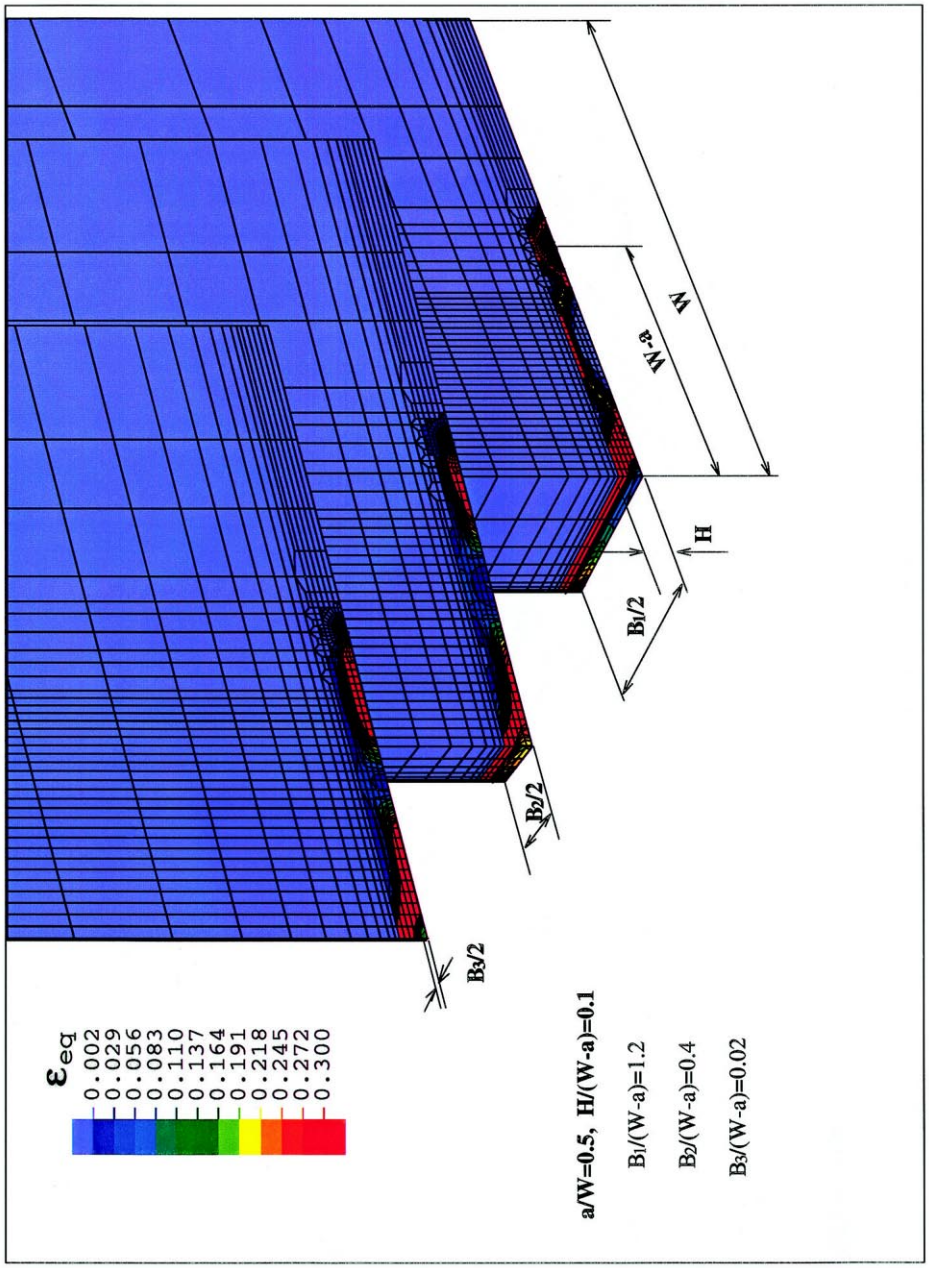

Fig. 14. Plastic strain distribution in the middle section of deeply undermatched bending specimens with various thicknesses.

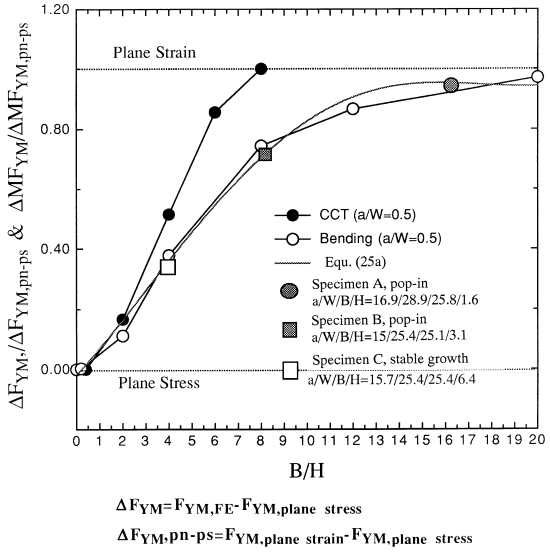

Fig. 15. Relationship between the yield moment and yield load, respectively, and the ratio B/H (thickness/half welded joint height); bending and tension cases; the CCT specimen is from Hao et al. (1997), specimens A, B, and C are from Reuter et al. (1994).

$$\Delta MF_{\mathrm{YM}} = \frac{MF_{\mathrm{YM,\ planes\ strain}} - MF_{\mathrm{YM,\ planes\ stress}}}{MF_{\mathrm{YM,\ planes\ stress}}}$$

for the case $B/H \geq 20$

$$MF_{\mathrm{YM}} = MF_{\mathrm{YM,\ plane\ strain}} \tag{25b}$$

The calculated limit moments for these seven thicknesses are displayed in Fig. 15, on which several examples of CCT specimens from Hao et al. (1994a, 1994b) are also plotted. Both tension and bending configurations exhibit an S-like dependence on thickness. However, when $B/H \geq 8$ the yield load for the tension specimens is almost equal to that in plane strain condition. For the bending configuration, the plane strain dominance occurs at $B/H \geq 20$. More numerical analyses are necessary to investigate the effect of thickness on the fracture behaviour of mismatching specimens.

6. Discussion

The findings presented in this paper are similar to those reported in our previous paper on the CCT geometry (Hao et al., 1997). It could again be demonstrated that the slip-line theory is a powerful tool for determining local stresses (see Figs. 5, 7(b) and 8) and yield loads (see Figs. 7(a) and 11) if the material under consideration can be regarded as deforming in an ideally plastic manner. It remains to be determined how strain hardening will affect these results. From the local stresses the constraint condition in terms of Q can be derived. Thus, essential items of the mechanical behaviour of a cracked mismatched component can be quantitatively formulated employing relatively simple slip-line models.

The stress peak found by Hao et al. (1997) ahead of the crack tip in the tensile loaded undermatched configuration was also found under bending loading, Fig. 8. In addition, on the compression side of the bend bar a second peak of about the same magnitude — now as a compressive stress — was observed. This stress pattern shows — although due to the presence of the crack — that a risk of failure in an

undermatched component should be considered at locations remote from the crack tip. This is emphasized by the strain pattern depicted e.g., in Figs. 8, 10 and 12(b).

Interesting support for these conclusions is given by the experimental work by Reuter et al. (1994); decreasing H for a given thickness of undermatched bend specimens, hence increasing B/H, created constraint conditions approaching plane strain, Fig. 15. As a consequence, failure of a specimen with a low B/H value took place by stable crack growth, whereas two specimen with larger B/H values exhibited failure initiation ahead of the crack tip followed by pop-in, Fig. 15.

As long as plastic deformation remains confined to the weld metal, i.e. as long as 'extreme undermatching' is realized, the yield load increases with the normalized ligament length, $(W-a)/H$, Fig. 7(a). The increase, however, is substantially lower than under tension, see Fig. 9 in Hao et al. (1997). As an example, at $(W-a)/H=10$ under bending the mismatch yield load is about 1.4 times that of a homogeneous weld metal bend bar, whereas tensile loading gives rise to a factor of 2.4 fold elevation of the mismatched yield load compared to the homogeneous weld metal case. This is due to the different slip-line geometries: under bending the slip lines expand much less in the lateral direction (perpendicular to the crack plane) than under tension so that the restraint exerted by the stiff base metal has a lesser effect on the slip line expansion.

Looking at the 3D behaviour, tensile loading leads to more rapid approach to plane strain with increasing thickness than bending loading, Fig. 15.

Finally, the decay of the mismatch effect on the yield load of overmatched welds with increasing $(W-a)/H$, Fig. 11, is very close to the behaviour of tensile loaded plates, see Fig. 18 in Hao et al. (1997). In both cases, for $(W-a)/H \geq 10$ the yield load is dominated by the base metal properties. Similarly, under both loading conditions undermatched welds are more dominated by the weld metal.

7. Conclusions

1. Plane strain and plane stress slip-line solutions for a pure bending specimen with different $(W-a)/H$ values and different degrees of mismatch have been constructed. From these solutions formulas for the limit moment and the constraint parameter Q have been established. They can be expressed in simple analytical form and can easily be used for application.
2. A high level of yield strength undermatch leads to a higher constraint at the crack tip even under net-section yielding condition. This increase depends on the ratio of thickness to weld metal height $(2H)$ as well as on the ratio of ligament length to $2H$. However, the amplitude of this elevation for the bending configuration is not as high as that in the tension case, because in a homogeneous bend bar there is already a higher constraint.
3. The effect of thickness on the pure bending configuration with an extremely undermatched welded joint has been investigated. Based on the 2D slip-line solutions and the 3D numerical analyses, a relation for estimating the yield load has been suggested. A prediction from this relation coincides with test results by Reuter et al. (1994).

Acknowledgements

The authors gratefully acknowledge the support by the German Science Foundation (Deutsche Forschungsgemeinschaft, Project B6 of the Sonderforschungsbereich 371).

Appendix A

In Fig. 16 the line L is an interface and the superscript 'I' or 'II' represents the quantity in either material. Consider an infinitesimal element on L, from the stress continuity condition we have:

$$\sigma_n^{\mathrm{W}} = \sigma_n^{\mathrm{B}}; \quad \tau_n^{\mathrm{W}} = \tau_n^{\mathrm{B}} \tag{A1}$$

and it is allowed to set

$$\sigma_t^{\mathrm{B}} \neq \sigma_t^{\mathrm{W}} \tag{A2}$$

which represents the discontinuity of the transverse stress over the interface L.

From the equilibrium condition at both materials we have the relation

$$\sigma_n^{\mathrm{B}} = \sigma_{\mathrm{m}}^{\mathrm{B}} - \frac{\sigma_{\mathrm{YB}}}{\sqrt{3}} \sin 2\left(\theta^{\mathrm{B}} - \eta\right); \quad \tau_n^{\mathrm{B}} = \cos 2\left(\theta^{\mathrm{B}} - \eta\right) \tag{A3a}$$

and

$$\sigma_n^{\mathrm{W}} = \sigma_{\mathrm{m}}^{\mathrm{W}} = -\frac{\sigma_{\mathrm{YW}}}{\sqrt{3}} \sin 2\left(\theta^{\mathrm{W}} - \eta\right); \tau_n^{\mathrm{W}} = \cos 2\left(\theta^{\mathrm{W}} - \eta\right) \tag{A3b}$$

where θ denotes the helix angle of an α family slip-line, σ_{m} is the mean stress, σ_{Y} represents the yield strength of the material and η is the angle between the normal vector of the interface and the x_1-coordinate (see Fig. 16).

Substituting Eqs. (A3a) and (A3b) in Eq. (A1) the following conditions of the stress components for a slip-line field across an interface can be obtained:

$$\sigma_{\mathrm{m}}^{\mathrm{B}} - \frac{\sigma_{\mathrm{YW}}}{\sqrt{3}} \sin 2\left(\theta^{\mathrm{W}} - \eta\right) = \sigma_{\mathrm{m}}^{\mathrm{W}} - \frac{\sigma_{\mathrm{YW}}}{\sqrt{3}} \sin 2\left(\theta^{\mathrm{W}} - \eta\right) \tag{A4a}$$

and

$$\frac{\sigma_{\mathrm{YB}}}{\sqrt{3}} \cos 2\left(\theta^{\mathrm{B}} - \eta\right) = \frac{\sigma_{\mathrm{YW}}}{\sqrt{3}} \cos 2\left(\theta^{\mathrm{W}} - \eta\right) \tag{A4b}$$

For the bi-material system shown in Fig. 9, the horizontal line is taken as x_1-coordinate so that

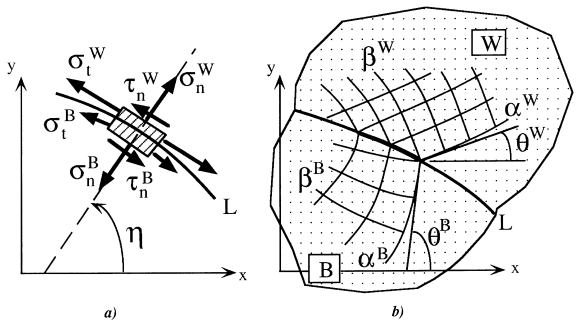

Fig. 16. Illustration of the connection conditions of slip-line fields across an interface.

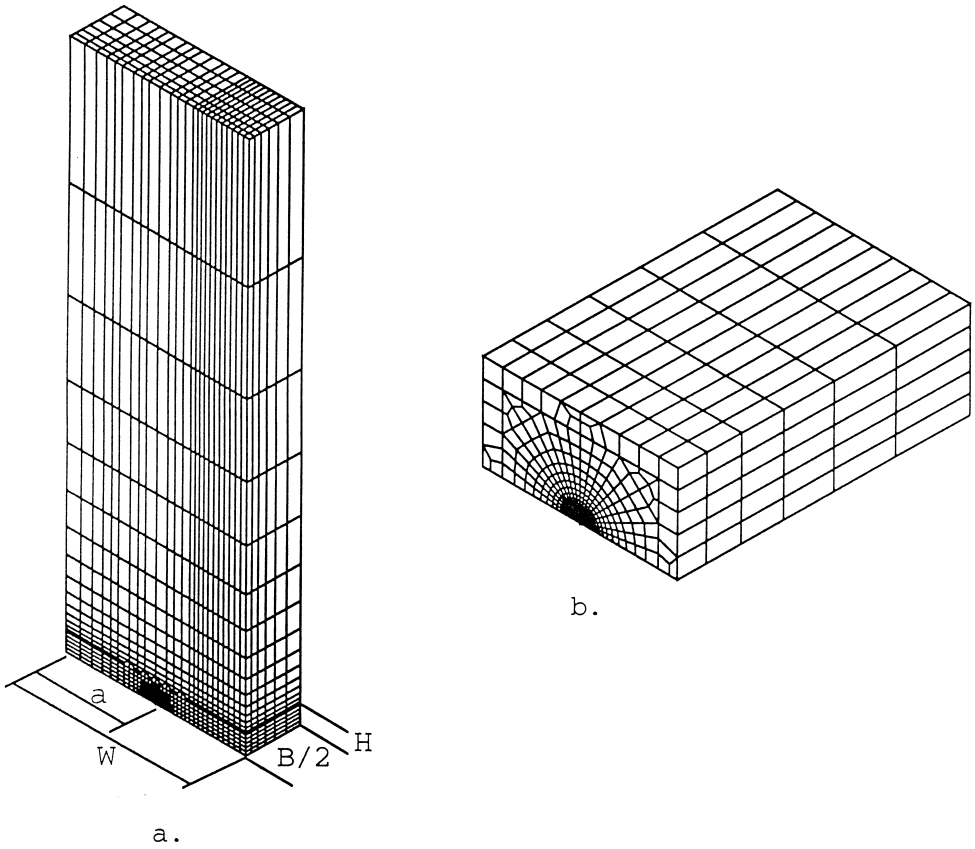

Fig. 17. A typical 3D finite element mesh.

$$\eta = 0 \tag{A5}$$

The kinematical permitted displacement field requires:

$$\theta^{W} = \theta^{B} \tag{A6}$$

Thus the necessary conditions for a slip-line penetrating an interface are

$$\theta^{W} = \theta^{B} = 45^{\circ} \tag{A7a}$$

and

$$\left[\frac{\sigma_{11}^{B} + \sigma_{22}^{B}}{2}\right] = \left[\frac{\sigma_{11}^{W} + \sigma_{22}^{W}}{2}\right] - \frac{\sigma_{YW}}{\sqrt{3}} + \frac{\sigma_{YB}}{\sqrt{3}} \tag{A7b}$$

The finite element techniques used are the same as described by Hao et al. (1997). A typical 3D mesh is shown in Fig. 17.

References

British Standard Institution, 1991. Guidance on Methods for Assessing the Acceptability of Flaws in Welded Structures. Published Document PD-6493.

Burstow, M.C., Ainsworth, R.A., 1995. Comparison of analytical, numerical and experimental solutions to problems of deeply cracked welded joints in bending. Fatigue Fract. Engng. Mater. Struct 18, 221–234.

Ewing, D.J.F., Hill, R., 1967. The plastic constraint of V-notched tension bar. Journal of M. P. S 16, 115.

Gilles, Ph., Franco, Ch., 1994. A new J-estimation scheme for cracks in mis-matching welds — the Aramis method. In: Mis-Matching of Welds, ESIS 17, Proceedings of Mis-Match 93 (May, 1993, Reinstorf, Germany). Mechanical Engineering Publications, London, 661.

Hao, S., Cornec, A., Schwalbe, K.-H., 1994a. On the crack driving force and constraint state in a mis-matched welded plate under tension. In: Proceeding of ECF 10, vol. 2, 1117.

Hao, S., Cornec, A., Schwalbe, K.-H., 1994. Investigation of the effect of thickness on the constraint state and yield loads of the mismatched weld: 2D and 3D analysis, IIW. Document, X-F-014-1994, presented in the Workshop of IIW subcommission X-F, Paris.

Hao, S., Cornec, A., Schwalbe, K.-H., 1995, unpublished results.

Hao, S., Cornec, A., Schwalbe, K.-H., 1997. Plastic stress–strain fields and yield loads of a plane strain cracked tensile panel with a mismatched welded joint. Int. J. of Solids and Structures 34, 297.

Hill, R., 1951. The Mathematical Theory of Plasticity. Oxford.

Hundy, B.B., 1954. Plane plastic. Metallurgia 49, 109.

Hutchinson, J., 1968. Plastic stress and strain fields at a crack tip. J. Mech. Phys. Solids 16, 337.

Joch, J., Ainsworth, R.A., Hyde, T.H., 1993. Yield load and J-estimates for idealised problems of deeply cracked welded joints in plane strain bending and tension. Fatigue Fracture Engng. Mater. Structures 16, 1061.

Joch, J., Ainsworth, R.A., 1994. Relationships between the J-integral and the crack tip opening displacement for stationary cracks in weldments at plastic collapse. Fatigue Fracture Engng. Mater. Structures 17, 1175.

Joch, J., Ainsworth, R.A., Hyde, T.H., Neale, B.K., 1994. Fracture parameters and fracture assessment for welded structure. In: Mis-Matching of Welds, ESIS 17, Proceedings of Mis-Match 93 (May, 1993, Reinstorf, Germany). Mechanical Engineering Publications, London, 609.

Kumar, V., German, M.D., Shih, C.F., 1981. An engineering approach for elastic–plastic fracture analysis. EPRI, Report NP-1931.

Milne, I., Ainsworth, R.A., Dowling, A.R., Stewart, A.T., 1986. Assessment of the integrity of structures containing defects. R/H/R6, Rev. 3, CEGB.

Nagtegaal, J.C., Parks, D.M., Rice, J.R., 1974. On numerical accurate finite element solutions in the fully plastic range. Comp. Meths. Appl. Mech. Engng 4, 153.

O'Dowd, N., Shih, C.F., 1992. Family of crack-tip fields characterized by a traxiality parameter-II. Fracture application. J. of Mech. Phys. of Solids 40, 939.

Prandtl, L., 1923. Anwendungsbeispiele zu einem Henckyschen Satz über das plastische Gleichgewicht. Z. Angew. Math. Mechanik 3 (6), 401.

Reuter, W.G., Ganti, S., Parks, D.M., Epstein, J.S., Lloyd, W.R., 1994. Elastic–plastic constraint in simulated butt welds. In: presented at the 26th National Symposium on Fracture Mech. ASTM, Philadelphia.

Schwalbe, K.-H., 1992. Effect of weld metal matching on toughness requirements: some simple analytical considerations using the Engineering Treatment Model (ETM). Int. J. of Fracture 56, 257.

Schwalbe, K.-H, Hao, S., Cornec, A., 1994. ETM-MM-the engineering treatment model for mis-matched welded joints. In: Mis-Matching of Welds, ESIS 17, Proceedings of Mis-Match 93 (May, 1993, Reinstorf, Germany). Mechanical Engineering Publications, London, 539.

Timoshenko, S.P., Goodier, J.N., 1970. Theory of Elasticity, 3rd ed. McGraw-Hill, New York, p. 90.

Wang, Y.Y., Kirk, M.T., Gordon, J.R., 1996. A comprehensive review of fracture toughness estimation procedures for mismatched specimens. In: 2nd Int. Symp. on Mis-Matching of Welds, April 24–26, Reinstorf-Lüneburg, Germany.